

# Mechanical Buckling: Mechanics, Metrology, and Stretchable Electronics

By Dahl-Young Khang, John A. Rogers, and Hong H. Lee\*

Mechanical buckling usually means catastrophic failure in structural mechanics systems. However, controlled buckling of thin films on compliant substrates has been used to advantage in diverse fields such as micro-/nanofabrication, optics, bioengineering, and metrology as well as fundamental mechanics studies. In this Feature Article, a mechanical buckling model is presented, which sprang, in part, from the buckling study of high-quality, single-crystalline nanomaterials. To check the mechanical-buckling phenomenon down to the nano-/molecular scale, well-aligned single-walled carbon nanotube arrays and cross linked carbon-based monolayers are transferred from growth substrate onto elastomeric substrate and then they are buckled into well-defined shapes that are amenable to quantitative analysis. From this nano- or molecular-scale buckling, it is shown that the mechanical moduli of nanoscale materials can easily be determined, even using a model based on continuum mechanics. In addition, buckling phenomena can be utilized for the determination of mechanical moduli of organic functional materials such as poly(3-hexylthiophene) (P3HT) and P3HT/6,6-phenyl-C<sub>61</sub>-butyric acid methyl ester (PCBM) composite, which are widely used for organic transistors and organic photovoltaics. The results provide useful information for the realization of flexible and/or stretchable organic electronics. Finally, the fabrication and applications of “wavy, stretchable” single-crystal Si electronics on elastomeric substrates are demonstrated.

stretched in one direction. Dried skins of fruits, such as apples, have wrinkles on their surfaces. Yet another common example of wrinkling is in aging human skin. All such phenomena originate from the same mechanism, i.e., mechanical buckling or wrinkling, although the detailed stress distributions may differ significantly. This article deals with the buckling system that comprises thin films on compliant substrates.

Since the pioneering work of Whitesides and co-workers at Harvard University,<sup>[3]</sup> there has been much interest in buckling, in controlled strategies for applications. In their work, vacuum-deposited (using e-beam evaporation) thin films of metals such as Au, Al, and Ti typically on an elastomeric substrate of polydimethylsiloxane (PDMS) were buckled into sinusoidal surface undulation. The thermal expansion of PDMS during deposition and then shrinkage to its initial dimension by cooling back to room temperature after the film deposition induces compressive stresses on the films. To relieve the stress, the metal film buckles into a wavy, sinusoidal shape. When deposited on a flat, unstructured substrate, the buckling

takes place randomly, i.e., with no preferential orientational order. This randomly buckled metal surface appears frosted, due to the light scattering from a network of periodic surface waves. By using bas-relief-patterned PDMS substrate, however, well-aligned, uniform buckling patterns could be obtained. The asymmetric distributions of stress in the  $x$ - $y$  plane lead to the ordering of buckling waves in one particular direction. The periodicity of the wave, or their wavelength, depends upon the film thickness and/or mechanical properties of materials involved in the system. This controlled buckling opens a new research direction in buckling, not as a nuisance but as a possibly very useful tool in many applications. Some of its useful application examples such as metrology and stretchable electronics, will be discussed in detail later in this article.

A similar yet slightly different buckling system, which has been studied in detail by Lee and co-workers at SNU,<sup>[4–10]</sup> represents another example of controlled buckling. A thin polymer layer that is confined between substrate and a thin metal capping layer leads to a wrinkled surface due to elastic mismatch when heated above the glass-transition temperature,  $T_g$ . Contacting a

## 1. Introduction

Buckling (also called “wrinkling”) is ubiquitous in our daily life.<sup>[1,2]</sup> It is common to find that a thin plastic sheet wrinkles when

[\*] Prof. H. H. Lee  
School of Chemical and Biological Engineering  
Seoul National University  
Seoul 151-742 (Korea)  
E-mail: honghlee@snu.ac.kr  
Prof. J. A. Rogers  
Department of Materials Science and Engineering  
University of Illinois at Urban-Champaign  
Urbana, IL 61801 (USA)  
Prof. D. Y. Khang  
Department of Materials Science and Engineering  
Yonsei University  
Seoul 120-749 (Korea)

DOI: 10.1002/adfm.200801065

patterned elastomeric stamp made of PDMS guides the buckling process by the physical confinement effect. If the periodicity of patterns on the stamp is comparable to that of given metal/polymer/substrate buckling system, the spontaneous wrinkling patterns could be assembled into a shape imposed by an elastomeric stamp, thus called physical self-assembly.<sup>[4]</sup> The wrinkled surface has rounded, smooth edges due to bending-energy cost of thin metal film, while the stamp used has rectangular, sharp edges. These rounded surface profiles may be found to be very useful in the fabrication of various optical surfaces. It was also shown that wave shape control is possible by changing the periodicity of patterns on the stamp relative to the intrinsic wavelength of given metal/polymer bilayer system.<sup>[6]</sup> For example, if the pattern periodicity on the stamp is large compared to the intrinsic wrinkling wavelength, the waves split and yield multiple harmonics, leading to symmetric/asymmetric double and triple modes. Further, the control of wave phase was demonstrated by altering the work of adhesion between stamp and metal surface.<sup>[10]</sup> When an oxygen plasma-treated PDMS stamp is used, which has a strong adhesion with the metal surface, a convex wave or negative replica of the stamp surface is obtained. In contrast, a non-treated, bare PDMS stamp leads to a concave wave (positive replica of stamp surface). This “wave-phase controllability”, together with wave shape control, provides a versatile tool for controlling the morphology of the wrinkled surface, and could lead to novel applications in many fields such as optics and microfluidics.

It is worth mentioning that the fundamental studies on the wrinkling induced by the relaxation of the confined polymer layer lead to a deeper understanding of the role of thermophysical properties of polymers. Spinodal wrinkling<sup>[5]</sup> was found to occur when the metal/polymer bilayer was heated just above  $T_g$ , which originates from the elastic property of the polymer. On the other hand, the worm-like wrinkling,<sup>[8]</sup> which reveals viscous fluidic behavior of the polymer, was found to take place when the sample was heated well above  $T_g$ . A comprehensive map of the wrinkling morphology of metal/polymer system is constructed in Ref. [9]

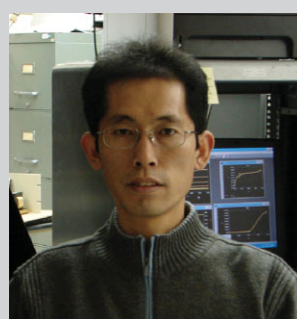
This article consists of three main sections. In Section 2, the mechanics of buckling will be discussed. The theoretical analysis of buckling at small strain, i.e., the conventional model, will be reviewed, followed by buckling analysis at large strain. The buckling experimental results with high-quality, single-crystalline material such as Si have led to a buckling model that is different from that of the small-strain case. Another interesting buckling system, delamination buckling, will also be introduced and analyzed. Then, two-dimensional buckling results are shown and discussed, including the width effect of the film on the buckling. In Section 3, examples of thin-film metrology based on buckling phenomena will be discussed. These include nano- or molecular-scale materials such as single-walled carbon nanotubes (SWNTs) and cross linked self-assembled monolayers (SAMs). Further, it will be shown that the mechanical moduli of common organic conductor/semiconductor materials, which are believed to be promising for low-cost, flexible electronics, can be determined by the buckling method. Section 4 is on the stretchable electronics application of the buckling. The buckled, wavy surface of metals, semiconductors, or electronic device layers will be shown to be reversibly stretchable. An externally applied stretching or compression on a buckled sample is accommodated as a change in the wave profile, without fracturing the layer, which

deteriorates the device performance. Also the two-dimensionally stretchable, fully functional circuits are introduced.

## 2. Buckling Mechanics

### 2.1. Thin-Film Buckling on Compliant Substrate: Small Strain

The buckling system under consideration here is schematically shown in Figure 1. A stiff, thin-film layer is prepared on a thick,



**Dahl-Young Khang** received his B.S. (1994), M.S. (1996), and Ph.D. (2000), all in Chemical Engineering, from the Seoul National University (SNU) under the supervision of Prof. Hong H. Lee. He then worked for a start-up company before joining Prof. John A. Rogers' group as a post-doctoral researcher in 2003. In 2008, he joined the Department of Materials Science and Engineering, Yonsei University as an assistant professor. His research focuses on soft electronics.



**John A. Rogers** obtained his B.A. and B.S. degrees from the University of Texas, Austin, in 1989. From MIT, he received S.M. degrees in 1992 and his Ph.D. in physical chemistry in 1995. From 1995 to 1997, Rogers was at the Harvard University;

he then worked at Bell Laboratories until 2002. He subsequently joined the faculty at University of Illinois at Urbana-Champaign. Rogers' research includes fundamental and applied aspects of nano- and molecular-scale materials.



**Hong H. Lee** received his B.S. in Chemical Engineering from the Seoul National University (SNU in 1966) and Ph.D. from Purdue University in 1971. After working for Westvaco Corporation for six years, he joined the University of Florida. In 1992, he moved to SNU

and was the director of the Nanoelectronics Institute from 1997 to 2001. His current research efforts are centered on two areas: unconventional nanolithographies and organic devices.

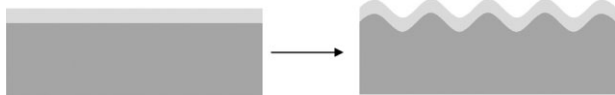


**Figure 1.** Schematic drawing for the buckling of a thin film on a compliant substrate.

less stiff substrate. When the sample is compressed, the film buckles into a sinusoidal shape to relieve the applied stress. The goal of the theoretical analysis of the buckling system is to find the buckling wavelength and amplitude. In general, a stiff film favors long wavelength when buckled, because it costs less energy than buckling into a rather short wavelength. On the other hand, the soft substrate favors shorter wavelength due to its lower energy cost. When combined, the buckling yields a value somewhere between these large and small wavelengths.

It is known that the energy method is very useful for non-linear buckling analysis.<sup>[11,12]</sup> By minimizing the total energy of the system (membrane and bending energies of film material, and deformation energy of substrate) with respect to the wavelength ( $\lambda$ ) and amplitude ( $A$ ), the following wavelength and amplitude result:

$$\lambda_0 = 2\pi h \left( \frac{\bar{E}_f}{3\bar{E}_s} \right)^{1/3}, \quad A = h \sqrt{\frac{\varepsilon_{\text{pre}}}{\varepsilon_c} - 1} \quad (1)$$

Here,  $\varepsilon_c = 0.25(3\bar{E}_s/\bar{E}_f)^{2/3}$  is the critical or minimum strain that is necessary for the buckling to occur,  $h$  the film thickness, and  $\bar{E}$  is the plane-strain moduli. The subscripts  $f$  and  $s$  denote film and substrate, respectively.

Note that the buckling wavelength depends only on the mechanical properties (Young's modulus and Poisson ratio) of the materials involved and the film thickness,  $h$ ; it does *not* depend on the prestrain. Also, the wavelength and amplitude are linearly proportional to the film thickness. Finally, the amplitude increases with applied strain quadratically. That is, the prestrain is absorbed by the increase in the wave amplitude, while the buckling wavelength

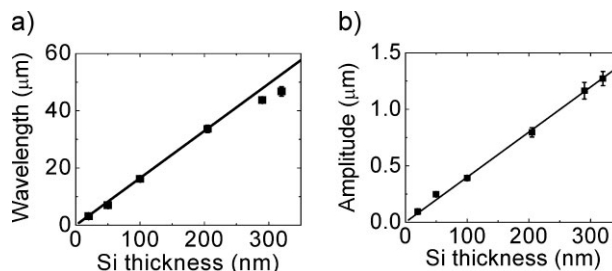


**Figure 2.** a) Buckling wavelength, and b) amplitude of wavy Si ribbons (100 nm thick, 20  $\mu\text{m}$  wide, and spaced 20  $\mu\text{m}$  apart) on PDMS substrate as a function of Si thickness. The lines are from buckling theory, given in Equation (1). Reproduced with permission from Ref. [13].

remains constant, which is contrary to our intuition. When the wavy, sinusoidal surface is compressed from both ends, the wavelength should become smaller according to our daily experience. It will be shown later that this is due to large deformation of substrate, which is not considered in the derivation above. Nevertheless, the above equations agree reasonably well with experiments if the applied strain is rather small, say smaller than  $\sim 5\%$ .

Figure 2 shows a comparison between small-strain theory Eq. (1) and experimental data for the buckling of single-crystalline Si ribbons on elastomeric PDMS.<sup>[13]</sup> In this case, the prestrain was in the range of 1–3%, which justifies the use of the above small-strain theory. It can be seen in the figure that both the buckling wavelength and the amplitude increase linearly with the film thickness.

## 2.2. Thin-Film Buckling on Compliant Substrate: Large Strain

In the buckling of single-crystal Si on PDMS substrate, it was found that the buckling wavelength decreases with increasing prestrain, as shown in Figure 3a. Here, the prestrain for the buckling ranged from  $\sim 0.5$  to  $\sim 30\%$ . This prestrain dependence of buckling wavelength was shown to be successfully modeled both analytically and numerically.<sup>[14,15]</sup> For the large strain, the

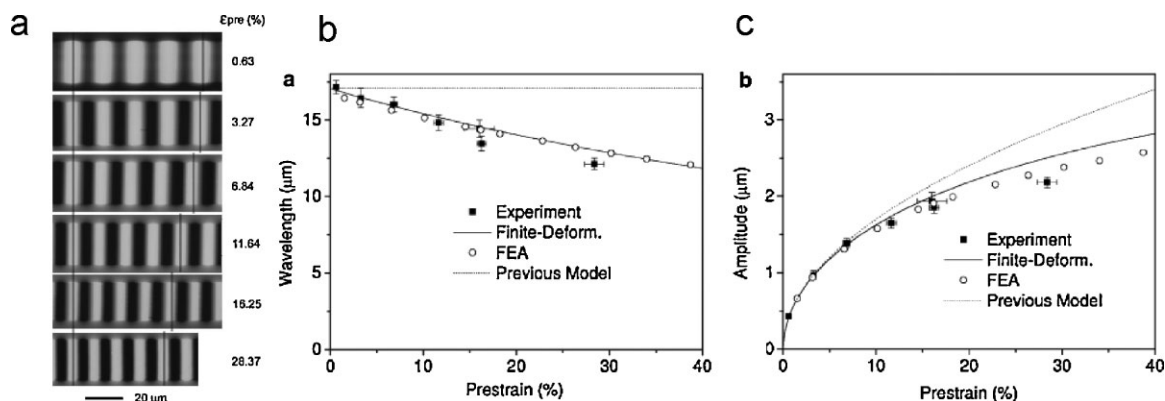


**Figure 3.** a) Stacked two-dimensional AFM images of buckled Si ribbons on PDMS, as a function of prestrain. The prestrain values are given at the right of each image in percent. The vertical lines are added to clearly show the wavelength change. The buckling wavelength decreases as the prestrain increases. b) Wavelength and c) amplitude of buckled Si ribbons on PDMS, as a function of prestrain. The new model based on finite deformation of substrate, Equation (2), agrees very well with both experiments and finite-element analysis. Also shown is the previous model based on small deformation, Equation (1), for comparison purposes. Reproduced with permission from Ref. [15].

elastomeric PDMS substrate becomes non-linear and thus modeled as neo-Hookean using the 2nd Piola–Kirchhoff stress formulation. From the system energy minimization as in Section 2.1, the new theory predicts the prestrain-dependent buckling wavelength and amplitude as follows:

$$\lambda = \frac{\lambda_0}{(1 + \varepsilon_{\text{pre}})(1 + \xi)^{1/3}}, \quad A = \frac{A_0}{\sqrt{1 + \varepsilon_{\text{pre}}(1 + \xi)^{1/3}}}, \quad (2)$$

$$\xi = \frac{5}{32} \varepsilon_{\text{pre}} (1 + \varepsilon_{\text{pre}})$$

Here,  $\lambda_0$  and  $A_0$  are the wavelength and amplitude, respectively, for the small-strain case, as given by Eq. (1). In the above equations,  $\lambda_0/(1 + \varepsilon_{\text{pre}})$  and  $A_0/(1 + \varepsilon_{\text{pre}})$  represent the change of  $\lambda$  and  $A$  resulting from simple accordion bellows mechanics, while the  $(1 + \xi)^{1/3}$  arises from the geometrical non-linearity (large deformation) and non-linear constitutive model for the substrate. Figure 3b and c shows a comparison between experimentally measured values of wavelength and amplitude and the new theory. Also plotted in the figure are the predictions from the small-strain theory and finite-element analysis. Both the new theory and finite-element analysis compare very well with the experimental data, while the small-strain model does not. For the buckling wavelength, the small-strain model predicts a constant, i.e., prestrain-independent, value. The discrepancy becomes significant for large values of prestrain. Finally, note that the new theory converges to the small-strain case when the prestrain value approaches zero. Therefore, it can be concluded that the small-strain model can still be applicable to the buckling system if the prestrain is small enough, up to  $\sim 5\%$  considering the experimental errors.

It might seem unusual that the previous buckling studies have relied only on the small-strain theory, considering its long history.<sup>[16,17]</sup> One possible explanation could be that the main object of previous buckling studies is to predict the critical buckling load, for the purpose of making sure that catastrophic collapse of structural members does not take place. In other words, it was not important at all whether the buckling wavelength depends on the prestrain or not. A high prestrain was simply to be avoided. Another possible explanation might lie in the material microstructure. The nearly perfect crystalline structure of Si films allows accurate measurement of the buckling profile at high prestrain values. Also, the strong chemical bonding between Si and PDMS surface resulting from UV/ozone or oxygen plasma made it possible to apply a large strain without delamination. In the meantime, the dominant film material for the buckling experiments since the work of Whitesides and co-workers has been the metal layer that was deposited by vacuum-evaporation techniques. These vacuum-deposited metals are in polycrystalline form. The material limitation and the main interest in preventing buckling are believed to be the reasons that the researchers worldwide have resorted to the small-strain theory for such a long time.

### 2.3. Controlled Delamination Buckling for Extreme Stretchability

The film delaminates off the substrate during compression unless the adhesion between them is strong enough. This delamination buckling is a very well known phenomenon in thin-film field, where

the delaminated buckled films takes the form of a tortuous shape, similar to the shape of telephone cord, thus called T-cord. The same situation occurs in the buckling of single-crystalline Si on PDMS substrate. Fortunately, the Si–O–Si bonding chemistry can be utilized. Typically, the PDMS surface is treated by UV/ozone exposure or by oxygen plasma treatment. These treatments are known to convert the PDMS surface into  $\text{SiO}_x$ , by removing the organic methyl groups in PDMS network. This modified, silica-like surface layer of PDMS can directly bond chemically with the thin Si ribbon. The Si ribbon popped off the surface if untreated bare PDMS is used, where only the weak van der Waals interaction is involved. The delamination of Si ribbons from PDMS substrate is in general uncontrollable, and thus it is considered to be a nuisance in buckling.

Controlled delamination, however, was shown to be possible when properly patterned PDMS is used.<sup>[18,19]</sup> In this approach, the bonding sites on the PDMS surface were selectively activated with UV/ozone treatment, while the other areas on PDMS remain inactive. The single-crystal ribbon elements of semiconductor materials such as Si and GaAs are then contacted with the chemically patterned PDMS substrate, which leads to piecewise chemical bonding between semiconductor ribbon and PDMS in the ribbon length direction. When the compressive strain is applied to this sample, the non-bonded regions of semiconductor ribbons are delaminated from the PDMS, forming an air-gapped bridge-like structure having periodic anchoring parts along the ribbon. The width of active/inactive parts can easily be controlled by changing the mask pattern that is used for patterned activation of PDMS surface.

Figure 4A illustrates this controlled delamination buckling process. The buckling profile can be expressed as:

$$w = \begin{cases} w_1 = \frac{1}{2}A \left(1 + \cos \frac{\pi x_1}{L_1}\right) \\ w_2 = 0 \end{cases} \quad (3)$$

where  $w_1$  and  $w_2$  denote the profiles of delaminated and bonded parts, respectively. Here, the buckling wavelength is already set during the selective surface activation step, while the amplitude is yet to be determined. In this delamination buckling case, the substrate does not deform significantly due to the delamination of film from the substrate surface. The substrate surface that has been in contact with the film before delamination remains stress free. Also the bonded regions of substrate remain flat after the relaxation of prestrain, as shown in the inset image of bottom panel of Figure 4a. Therefore, we need to take into account only film energies, i.e., membrane and bending energies, in the total system energy formulation.

Minimization of total energy with respect to the buckling amplitude gives:

$$A = \frac{4}{\pi} \sqrt{L_1 L_2 (\varepsilon_{\text{pre}} - \varepsilon_c)} \quad (4)$$

Here,  $\varepsilon_c = h^2 \pi^2 / 12 L_1^2$  is the critical strain for buckling, which is identical to the Euler buckling strain for a doubly clamped beam with length  $2L_1$  and bending rigidity of  $h^3 \bar{E}_f / 12$ . Figure 4b shows the comparison of buckling profiles obtained from

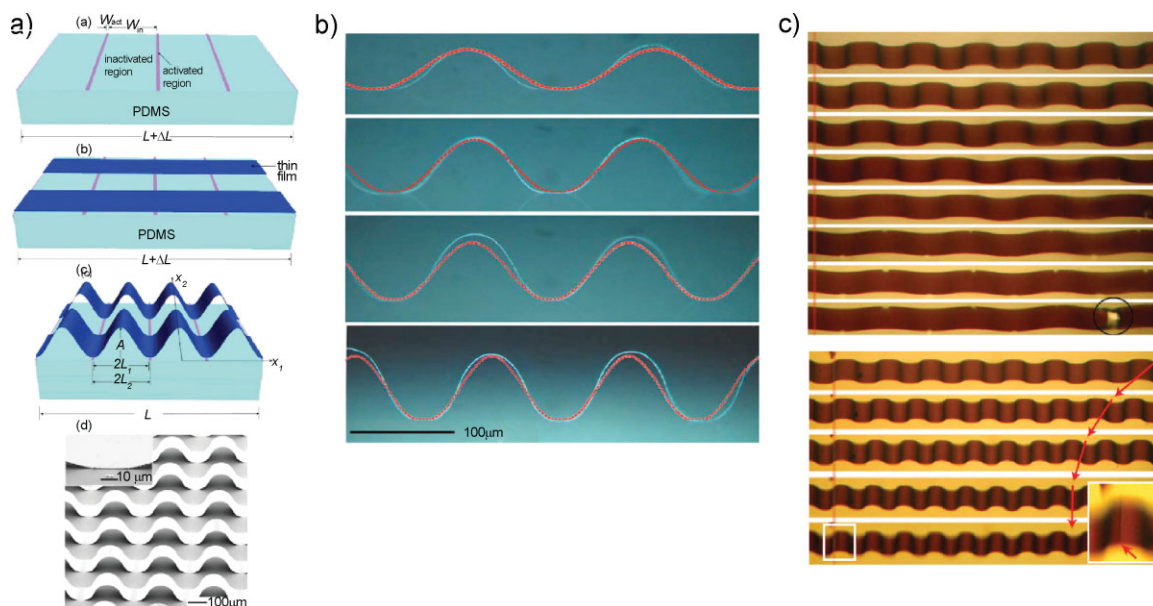


**Figure 4.** a) Schematic illustration of steps for controlled delamination buckling process. Prestretched PDMS substrate is selectively UV/ozone treated (or activated, purple colored areas).  $L$  is the initial length of PDMS,  $W_{in}$  and  $W_{act}$  are the length of inactivated and activated length, respectively. Bottom panel: SEM image of buckled GaAs film on PDMS by this approach. Inset shows the interface between GaAs film and PDMS, where no observable deformation of substrate PDMS is found. b) Comparison of buckling profiles between experiments and analytical solution, Equation (6), as a function of prestrain (from  $\sim 10$  to 56.0%, top to bottom). The GaAs thin ribbons are delamination-buckled with  $W_{in} = 190 \mu\text{m}$  and  $W_{act} = 10 \mu\text{m}$ . c) Optical micrographs of stretched (top, 0 $\sim$ 53%) and compressed (bottom, 0% $\sim$ 25%) GaAs ribbons, buckled and embedded in PDMS. Fracture of ribbon occurs at  $>50\%$  in tension, while  $>25\%$  in compression, thus enabling stretchability of  $\sim 100\%$ . Reproduced with permission from Refs. [18, 19].

experiments and theory. Good agreement between analytical solution and experiments can be seen.

The critical buckling strain,  $\varepsilon_c$ , is on the order of  $10^{-6}$  under the typical experimental conditions ( $L_1 \sim 100 \mu\text{m}$ ,  $h \sim 100 \text{nm}$ ). Therefore, the buckling amplitude in the above equation becomes

$$A \sim \frac{4}{\pi} \sqrt{L_1 L_2 \varepsilon_{pre}} \quad (5)$$

That is, the buckling amplitude is *independent* of materials properties (Young's modulus, thickness), and is completely determined by the geometry of selective surface treatment of PDMS substrate and the prestrain. Therefore, thin films of different materials will yield very similar buckling profiles, which were experimentally confirmed for Si and GaAs.

Considering the negligible membrane strain in the buckled film, the maximum strain in the buckled film is the bending strain that occurs at the wave peak. The bending strain can be calculated from the film curvature,  $\partial^2 w / \partial x^2$ . The modified length is typically much shorter than the non-treated one (i.e.,  $L_1 \approx L_2$ ), which further simplifies the above maximum strain to

$$\varepsilon_{max} \approx \frac{h\pi}{L_1} \sqrt{\varepsilon_{pre}} \quad (6)$$

For a 0.3- $\mu\text{m}$ -thick GaAs film buckled on a patterned PDMS substrate with  $W_{act} = 10 \mu\text{m}$ ,  $W_{in} = 400 \mu\text{m}$ , and  $\varepsilon_{pre} = 60\%$ , the

maximum strain in the buckled film is  $\sim 0.6\%$ , which is two orders of magnitude smaller than the prestrain. This enables the extreme stretchability of the delamination buckled films. Figure 4c shows this large stretchability, stretching up to  $\sim 60\%$  and compression to approximately  $-25\%$ , which amounts to almost 100% stretchability. Another unique feature of this approach lies in the extreme bendability. By embedding the delamination buckled thin films into PDMS, the film can be located at or near mechanical neutral plane, where there is no strain upon bending.

#### 2.4. Finite Width Effect in One-Dimensional Buckling and Two-Dimensional Buckling

For Si ribbons having finite width, the buckling wavelength and amplitude were found to depend upon their width. Figure 5b shows the plane-view AFM images of buckled Si ribbons on PDMS. Here, the ribbon width varies from 2, 5, 20, 50 to 100  $\mu\text{m}$ , from top to bottom. It clearly shows the increase in buckling wavelength with increasing ribbon width. In all existing mechanics models, it is assumed that the film width (dimension perpendicular to prestrain direction) is much larger than the wavelength such that the deformation is plane strain. This assumption is invalid when the film width becomes comparable or smaller than the buckling wavelength. To model this width-dependent buckling profile, the substrate deformation energy

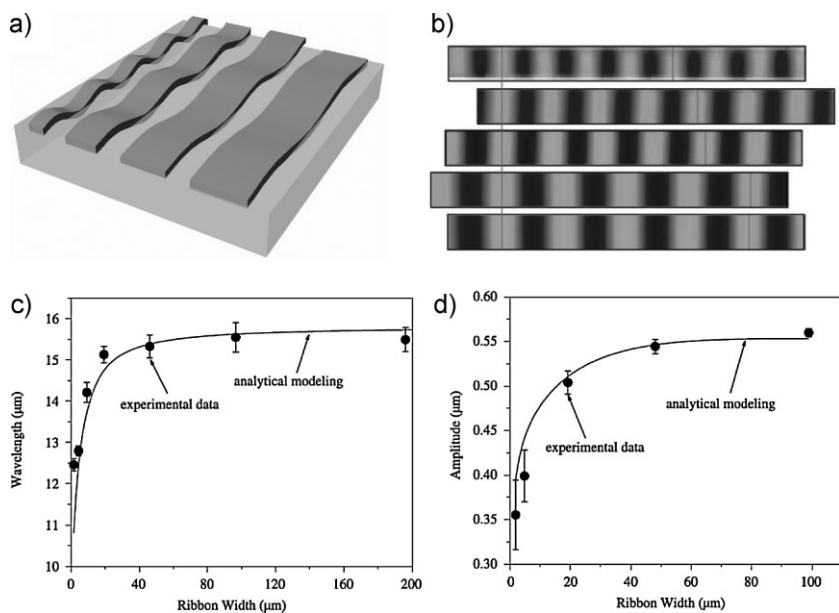


**Figure 5.** An schematic demonstration of width effect on buckling wavelength is shown in (a). Note that the narrower the ribbon, the shorter the buckling wavelength. b) Stacked AFM plane-view images of buckled Si (100 nm) ribbons with different widths of 2, 5, 20, 50, and 100 μm (from top to bottom). A wavepeak in each image is aligned at the left and marked with a long line, and their fourth wavepeaks are marked with short lines, indicating the variation of wavelength with respect to the ribbon width. The comparison between experiments and analytic modeling for width effect are shown in (c) and (d). Reproduced with permission from Ref. [20].

should be calculated in a way different from the previous solutions. The substrate deformation is confined under the region that is in contact with films, and other are as do not deform at all, except near the ribbon edge area. The deformation of substrate is integrated over the ribbon width using Boussinesq's solution, which contains modified Bessel and Struve functions in its solution. The calculated substrate energy contains film width in its formula, which explicitly reflects the film width effect on the buckling profile. On the other hand, the film energy, membrane and bending energy of the buckled film does not depend on the film width. From the energy minimization with respect to wavelength and amplitude, the width-dependent buckling wavelength and amplitude formula are derived in Ref. [20]. Figure 5c and d shows the comparison between theoretical model and experimental data on the width-dependent buckling. The developed model is shown to agree very well with the experiments.

From the width-effect analysis discussed above, it is natural to imagine that the buckling would be two-dimensional when the film width becomes large enough, that is, if the film is not a ribbon but a thin plate shape. This 2D buckling<sup>[21,22]</sup> is expected to endow stretchability in two -dimensions. In the 2D buckling, the buckling morphology changes depending on the two-dimensional stress state; stripe, zig-zag, and labyrinth patterns form as the sample position changes from edge to center region, as shown in Figure 6. Figure 7 shows the 2D stretchability of these 2D buckled Si nanomembranes.

values obtained by other methods. This buckling-based mechanical modulus measurement is especially well suited for thin-film materials, compared to other techniques such as conventional tensile test and nanoindentation, in that it does not need any expensive and complex equipment or bulk quantity of samples. Thus, it is very well suited for materials for which it is difficult or impossible to prepare bulk samples. Finally, the method is easy, fast, and less prone to experimental error because the wavelength can be averaged over the macroscopic dimension of the sample.

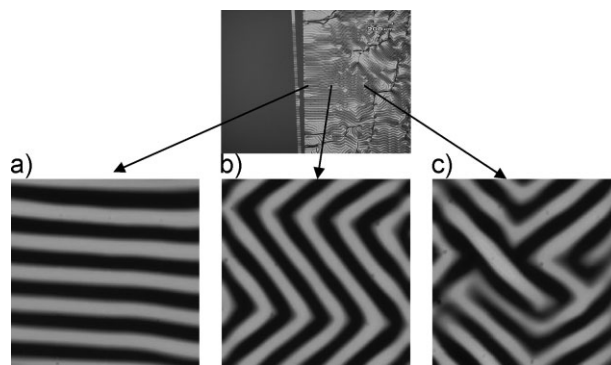


**Figure 6.** Various morphologies of two-dimensionally buckled Si (100 nm) nanomembrane on PDMS, at different positions on sample surface; stripes (a), zig-zag or herringbone (b), and labyrinth or random (c) buckling appears sequentially, from sample edge into inner region.

### 3. Buckling-Based Metrology

#### 3.1. Thin-Film Modulus Measurement by Buckling Analysis

The buckling wavelength equation derived in Section 2 can be rearranged to yield:

$$\bar{E}_f = 3\bar{E}_s \left( \frac{\lambda}{2\pi h} \right)^3, \quad \bar{E}_s = \frac{1}{3} \bar{E}_f \left( \frac{2\pi h}{\lambda} \right)^3 \quad (7)$$

Thus, the unknown Young's modulus of film material, for given mechanical properties of substrate and film thickness, can be extracted from the measurement of buckling wavelength. Similarly, the modulus of substrate can be measured by a similar approach. A group at NIST was the first to demonstrate this capability,<sup>[23,24]</sup> and they named it "strain-induced elastic buckling instability" for mechanical measurement, or SIEBIMM. The thin (150~250 nm) polystyrene (PS) film was prepared on PDMS substrate, and the wavelength of buckled surface was measured using optical microscopy. The measured wavelength values were used to calculate the Young's modulus of PS film from the above equation. The modulus values thus determined were almost constant for all film thicknesses investigated, and agreed well with literature values as well as with the

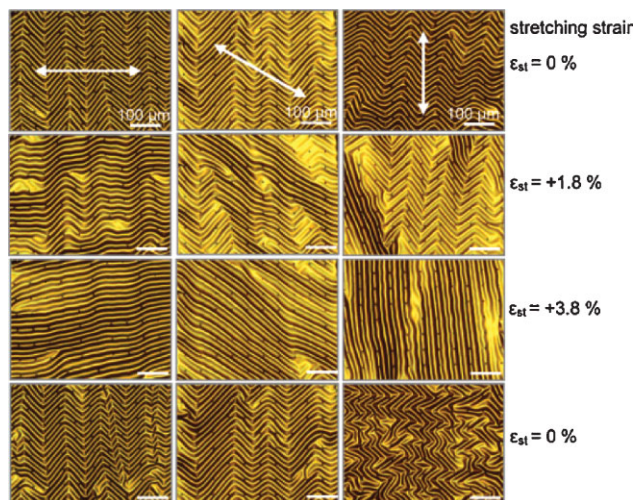


**Figure 7.** Optical micrographs of 2D wavy Si (100 nm) nanomembranes on PDMS under stretching into three different directions. The white arrows in the top frames denote the stretching direction, and the applied strain values are given next to rightmost images for each frame. Reproduced with permission from Ref. [21].

The mechanical modulus of polyelectrolyte multilayer (PEM) was also successfully determined using this method.<sup>[25,26]</sup> Also, the modulus of soft substrate was determined in a similar way.<sup>[27]</sup> Further, it was demonstrated that the modulus of nano- or molecular-scale materials such as SWNTs<sup>[28]</sup> and cross linked SAM<sup>[29]</sup> can be determined by the buckling method. Figure 8A shows the AFM image of the buckled, wavy SWNT arrays on PDMS. The buckling wavelength of SWNTs, which depends on the nanotube diameter, was measured by high-resolution AFM and plotted in Figure 8B. Fitting the measured dependence of wavelength on tube diameter has led to Young's modulus of SWNT of  $1.3 \pm 0.2$  TPa, which is in quantitative agreement with the reported literature values.

### 3.2. Mechanical Modulus of Functional Organics

Recently, there has been a lot of effort to use organic materials such as conducting or semiconducting polymers and oligomers, for flexible electronics. It is important to know the mechanical properties of the materials involved in flexible applications, which would be needed to design fabrication processes such as roll-to-roll schemes and to study the mechanical behavior of final products during service. In general, however, it is not easy or realistic to make these organic materials into a bulk form for mechanical tests. In particular, these materials are used as a film in electronics applications and therefore, the buckling-based mechanical characterization of these materials should be particularly useful.

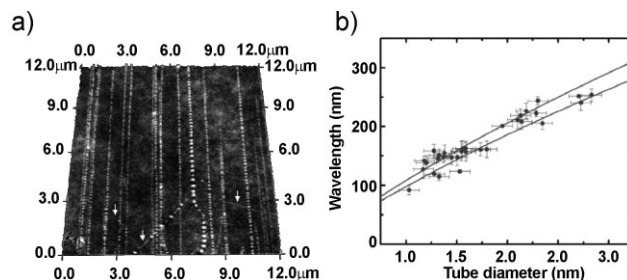


**Figure 8.** Modulus measurement of SWNTs by buckling. a) AFM image of buckled SWNTs on PDMS. b) Comparison between experimentally measured buckling wavelengths and calculation (gray lines). The modulus of SWNT is calculated to be  $1.3 \pm 0.2$  TPa. Reproduced with permission from Ref. [28].

As an example, we determined the Young's modulus of poly(3-hexylthiophene) (P3HT) and its blend with fullerene derivative, 6,6-phenyl-C<sub>61</sub>-butyric acid methyl ester (PCBM).<sup>[30]</sup> P3HT has been widely used as an active semiconductor material in organic field effect transistor (OTFT), while P3HT/PCBM composite shows good photovoltaic conversion efficiency in a bulk heterojunction (BHJ) form. These organic electronic devices can be fabricated on plastic substrate such that the final product can be bendable. The P3HT or P3HT/PCBM film was spun on glass substrate, on which fluorinated SAM (F-SAM) was coated. The film on glass could be easily picked-up onto PDMS, due to conformal contact of PDMS and low adhesion of film on the SAM-coated glass. The picked film/PDMS was loaded on a home-made stage and buckled by compression. Figure 9a (pure P3HT) and 9c (P3HT/PCBM blend)

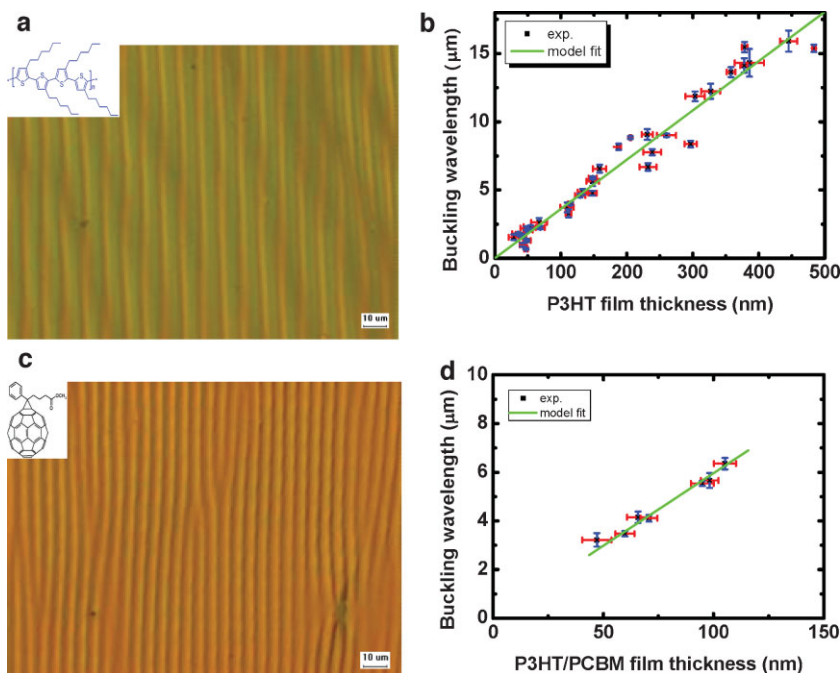


**Figure 9.** Mechanical modulus of P3HT and P3HT/PCBM films. Optical microscopy images for buckled P3HT and P3HT/PCBM films in (a) and (c), respectively. The insets show the chemical structure of P3HT and PCBM in the images. Measured wavelength data are plotted in (b) and (d), as a function of film thickness, where the green lines are fitted results.

shows the optical microscopy images of buckled films. The buckling wavelength was determined by measuring the distance between many waves (typically 10~20 waves) and dividing it by the number of waves contained within. This leads to a more accurate value than that from single wave measurement, because of averaging of many waves that have different wavelength values. Figure 9b and d shows the plot of wavelength as a function of film thickness, from which the mechanical modulus is extracted. The P3HT/PCBM blend has much larger, ~5 times, modulus (6.2 GPa) than that of pure P3HT (1.3 GPa). This high modulus of composite film may be attributed to the filler effect of PCBM nanoparticles.

It is well known that the detailed nanoscale morphology of P3HT/PCBM composite has significant effect on the solar cell performance.<sup>[31,32]</sup> The bi-continuous, nanoscale phase separated composite morphology yields a much higher solar cell efficiency than the random mixture, because the photogenerated carriers can be efficiently separated and collected when they move along continuous paths to the collecting electrodes. Therefore, it would be interesting to check if there is any difference in the mechanical property between phase-separated and random composites. For this, one set of P3HT/PCBM composite film samples was annealed at 100 °C for 3 h to induce the nanophase separation, while the other was not. The results (not shown here) showed that there is no noticeable difference in the mechanical modulus of composite films, irrespective of thermal annealing and thus nanophase separation.

## 4. Stretchable Electronics

### 4.1. Stretchable Metal Interconnection<sup>[33–36]</sup>

One of the direct applications of buckled thin film of metals on elastomeric substrate is the stretchable interconnection, that is, electrical connection among devices and/or devices to the outside world. Here, the devices may be stretchable itself, or they may be stiff. In the latter case, the elastomeric substrate would have rigid device islands interconnected by buckled metal layers on it, and thus the whole sample would be stretchable because an externally applied strain will mainly be absorbed by the buckled metal parts.

In this approach, a thin metal layer is deposited on a prestretched elastomeric substrate, in which the metal will be buckled into wavy, sinusoidal shape after the release of prestrain. As expected, the buckled film shows almost constant resistance up to ~100% degree

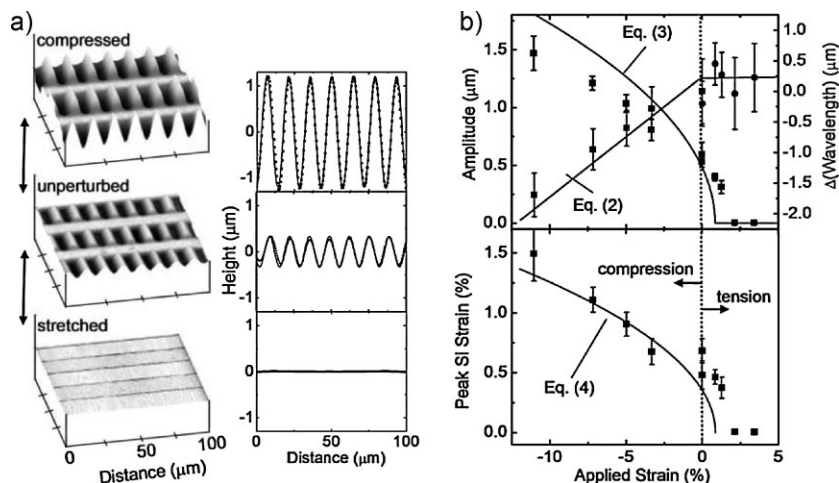


**Figure 10.** a) AFM images (left) and section profiles (right) of wavy Si ribbons on PDMS. The images correspond to compressed, unperturbed, and stretched state along the ribbon direction, from top to bottom. b) The change of wavelength (curved line) and amplitude (straight line) of wavy Si ribbons as a function of external strain (top). The maximum, or peak, strain as a function of external strain is shown in the bottom panel. Reproduced with permission from Ref. [13].

of stretching, which is mainly determined by the prestrain applied during film deposition. Also this process is reversible within experimental error. On the other hand, the flat metal film shows almost linear increase in resistance with stretching. As a real implementations of this stretchable interconnection, the amor-

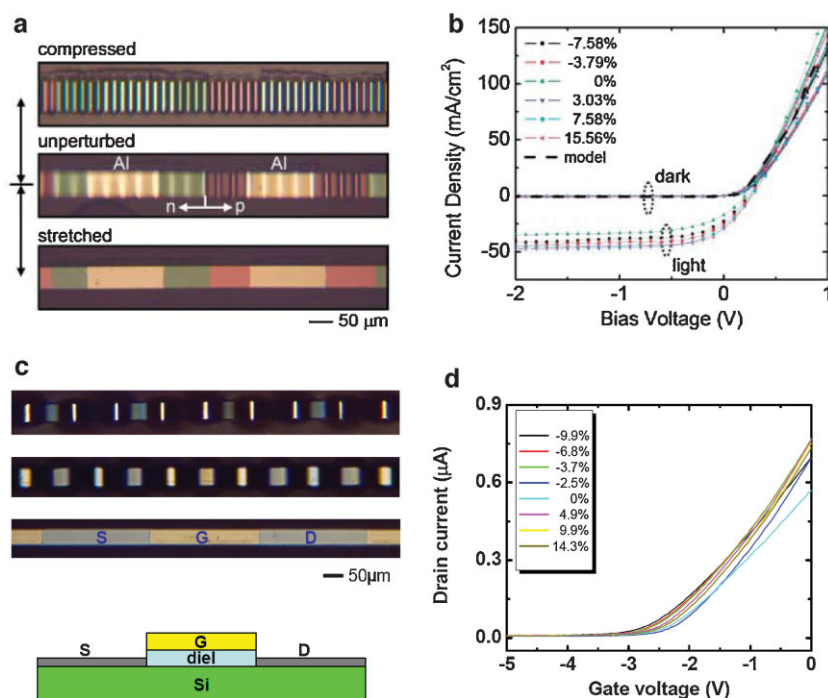


**Figure 11.** Examples of stretchable electronic devices. The optical microscopy images of buckled Si ribbons on PDMS, having pn-junction diodes and thin film transistors on them, for compressed, unperturbed, and stretched states, are shown in (a) and (c), respectively. The bottom part of (c) shows the structure of a transistor device, which is a self-aligned, Schottky metal-oxide-semiconductor field effect transistor (MOSFET). Reproduced with permission from Ref. [13].

phous Si thin-film transistors (TFTs) made on polyimide foil were faced down on contact pads forming inverter circuits, while the interconnection among them was made using buckled Au film. The buckled, wavy metal interconnection worked well even under the stretching, i.e., the whole circuit of rigid device islands connected by buckled metal still worked well under the stretching. This simple approach is expected to open the first market for stretchable electronics products such as hairband-type thermometer, and toys.

#### 4.2. High-Performance Stretchable Electronics Using Buckled Single-Crystal Inorganics

Although most inorganic, single-crystal semiconductor materials such as Si, GaAs, and InP are notorious for their brittleness, it was demonstrated that these materials are flexible enough to be used for bendable electronics, if they are made thin.<sup>[37–39]</sup> Therefore, it is expected that the thin-film form of these materials can also be made into wavy shape through buckling. The thin single-crystal Si layer was the first that was made into buckled, wavy shape, as already discussed in Section 2 in terms of buckling mechanics. For the stretchable applications, however, it is important to understand not only the initial buckling mechanics, but also the post-buckling mechanics. Here, the post-buckling mechanics has to do with the response of buckled material to an externally applied strain. Intuitively, one can surmise that the sinusoidal surface will change to one with different periodicity and amplitude when stretched or compressed, as shown in Figure 10a. In stretchable electronic applications, the maximum strain in the active semiconductor material is the most important factor to be considered, because the material will fracture or fail above a certain limit of strain. In an ideally sinusoidal buckled film, the maximum strain occurs at wave peaks or troughs where the curvature is the highest. Assuming that the surface profile is sinusoidal such that  $w = A \sin(2\pi x/\lambda)$ , the maximum strain is given by:

$$\varepsilon_{\max} = \frac{2\pi^2 Ah}{\lambda^2} \quad (8)$$

Because the fracture limit of typical inorganic semiconductors is around 2%, the maximum strain in the buckled material should be less than the fracture limit to prevent failure. In the example of Figure 10, the values of wavelength and amplitude are  $\sim 15$  and  $1 \mu\text{m}$ , respectively. Therefore, the maximum strain is  $\sim 1\%$ , while the applied strain is  $\sim 5\%$ . In other words, the active semiconductor material experiences substantially less strain than the externally applied strain, which makes stretching possible.

The fabrication of stretchable Si electronic devices is similar to that of wavy Si, except that the Si ribbon elements have additional layers such as dielectrics, and contact metals. All the high-temperature processing steps such as doping or thermal oxidation are usually done before the Si ribbons are transferred to elastomeric substrate, because the elastomeric substrate is incompatible with such high temperature steps. Then, the wet removal of underlying oxide layer releases the Si ribbons having device structure. Note that the devices are passivated to protect

them from wet etching chemicals prior to the etching. When picked up by PDMS substrate, however, the upside of the ribbons is down, which makes subsequent device characterizations impossible because the contact metals are now buried below the surface. To flip over the ribbons again, another piece of PDMS was used. A stickier form of PDMS, or partially cured PDMS, was used for this purpose.

As a simple example of stretchable Si electronics, two-terminal pn diodes and three-terminal field-effect transistors were fabricated and tested, as shown in Figure 11. In both cases, the initial wavy configuration could be reversibly converted to flat or wavier shape, upon stretching or compressing, respectively (Fig. 11a and c). Also, the devices were functioning well during and after the external straining. The scattering of data in Figure 11b and d is mainly due to irreproducible probe contact onto these devices; it is very difficult to make reliable and reproducible electrical contact on thin film devices that are fabricated on the very soft elastomeric substrate.

An alternative to 2D stretching is to use an ultrathin base layer with arbitrarily-shaped semiconductor elements, as shown in Figure 12.<sup>[40]</sup> Although the semiconductor elements are too small to have two-dimensional buckling characteristics as shown in

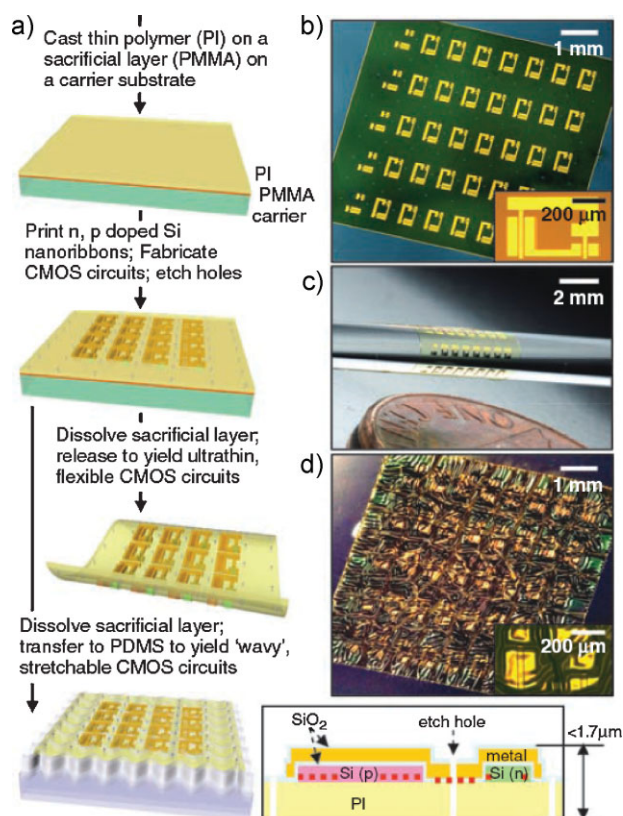


**Figure 12.** Schematic fabrication steps for two-dimensionally stretchable electronic devices (bottom frame of left column), and cross-sectional view with neutral mechanical plane indicated with a red dashed line (bottom frame of right column). The optical images of circuits on the carrier wafer (with single CMOS as an inset), on a thin rod, and in a wavy configuration on PDMS, are shown in (b), (c), and (d), respectively. Reproduced with permission from Ref. [40].

Figure 12, the ultrathin base layer that is supporting these elements can buckle in two-dimensional space when it is placed on prestretched elastomeric substrate. Using this approach, two dimensionally stretchable electronic circuits such as complementary metal/oxide/semiconductor (CMOS) and ring oscillator circuits are successfully demonstrated in Ref. [40].

## 5. Conclusions

In this article, we have demonstrated that the mechanical buckling phenomenon is no longer a problem to be avoided as in, for instance, structural mechanics. Rather, it is now finding novel applications in various fields. Some of them are a simple extension of or complement to existing technologies, while others can be whole new fields enabled by buckling.

Thin film form of materials is ubiquitous and now indispensable in modern society. The mechanical property of materials has long been determined on the basis of conventional testing protocols that need test specimens in bulk form. In contrast, the metrology for materials in thin film form has never been a simple task in itself. Furthermore, it is known that the mechanical property of thin film of a material may differ from that of bulk due to larger surface to volume ratio. In some other cases, a material cannot be easily prepared in bulk shape. In this light, the buckling-based determination of mechanical property of materials in thin film form is an invaluable addition, in that it is simple, fast, and easy to implement. It does not need any complex or expensive instruments. The results reported in this work, i.e., modulus of functional organic materials, exemplify the kinds of applications that can be made with the technique. Better understanding of mechanical characteristics of materials in thin film form would be very useful in emerging fields such as flexible electronics.

In the course of buckling study on single-crystal inorganic semiconductors such as Si, we have found that the conventional buckling model has limited capability. It could not explain the experimental results at large strain. The newly developed model, however, is shown to be applicable to large strain (up to ~30%), while it reduces to the conventional model at small strain. The well-defined single-crystalline microstructure of material has enabled to develop the general buckling model. In terms of enhanced stretchability, the delamination buckling using spatially controlled adhesion between film and substrate has been found to be very useful. The mechanics model for the delamination buckling can be applicable to any materials, which may open a variety of applications using stretchable form of various functional materials.

The application of buckled film on elastomeric substrate has led to the realization of stretchable electronics, which is more challenging than bendable ones. An example is the use of monocrystalline inorganic semiconductors, such as Si for the electronic devices in stretchable form, which perform well even under the external loading such as stretching or compression. This may open the way to various unprecedented applications in which the devices can conform to the objects having unusual form factor including wearable electronics. For this to be realized, however, extensive studies would be required.

## Acknowledgements

D.-Y. Khang acknowledges financial support from the Yonsei University Research Fund of 2008, and "System IC 2010" project of Korea Ministry of Commerce, Industry and Economy. This article is part of a special issue on Materials Science in Korea.

Received: July 25, 2008

Revised: October 10, 2008

Published online:

- [1] E. Cerda, L. Mahadevan, *Phys. Rev. Lett.* **2003**, *90*, 074302.
- [2] J. Genzer, J. Groenewold, *Soft Matter* **2006**, *2*, 310.
- [3] N. Bowden, S. Brittain, A. G. Evans, J. W. Hutchinson, G. M. Whitesides, *Nature* **1998**, *393*, 146.
- [4] P. J. Yoo, K. Y. Suh, S. Y. Park, H. H. Lee, *Adv. Mater.* **2002**, *14*, 1383.
- [5] P. J. Yoo, H. H. Lee, *Phys. Rev. Lett.* **2003**, *91*, 154502.
- [6] P. J. Yoo, S. Y. Park, S. J. Kwon, K. Y. Suh, H. H. Lee, *Appl. Phys. Lett.* **2003**, *83*, 4444.
- [7] S. J. Kwon, P. J. Yoo, H. H. Lee, *Appl. Phys. Lett.* **2004**, *84*, 4487.
- [8] P. J. Yoo, K. Y. Suh, H. Kang, H. H. Lee, *Phys. Rev. Lett.* **2004**, *93*, 034301.
- [9] P. J. Yoo, H. H. Lee, *Macromolecules* **2005**, *38*, 2820.
- [10] P. J. Yoo, H. H. Lee, *Langmuir* **2008**, *24*, 6897.
- [11] J. Groenewold, *Physica A* **2001**, *298*, 32.
- [12] Z. Y. Huang, W. Hong, Z. Suo, *J. Mech. Phys. Solids* **2005**, *53*, 2101.
- [13] D.-Y. Khang, H. Jiang, Y. Huang, J. A. Rogers, *Science* **2006**, *311*, 208.
- [14] H. Jiang, D.-Y. Khang, J. Song, Y. Sun, Y. Huang, J. A. Rogers, *Proc. Natl. Acad. Sci. USA* **2007**, *104*, 15607.
- [15] J. Song, H. Jiang, Z. J. Liu, D.-Y. Khang, Y. Huang, J. A. Rogers, C. Lu, C. G. Koh, *Int. J. Solids Struct.* **2008**, *45*, 3107.
- [16] S. P. Timoshenko, J. M. Gere, *Theory of Elastic Stability*, 2nd ed., McGraw-Hill, London **1961**.
- [17] H. G. Allen, *Analysis and Design of Structural Sandwich Panels*, Pergamon Press, London **1969**.
- [18] Y. Sun, W. M. Choi, H. Jiang, Y. Huang, J. A. Rogers, *Nat. Nanotechnol.* **2006**, *1*, 201.
- [19] H. Jiang, Y. Sun, J. A. Rogers, Y. Huang, *Appl. Phys. Lett.* **2007**, *90*, 133119.
- [20] H. Jiang, D.-Y. Khang, H. Fei, H. Kim, Y. Huang, J. Xiao, J. A. Rogers, *J. Mech. Phys. Solids* **2008**, *56*, 2585.
- [21] W. M. Choi, J. Song, D.-Y. Khang, H. Jiang, Y. Huang, J. A. Rogers, *Nano Lett.* **2007**, *7*, 1655.
- [22] J. Song, H. Jiang, W. M. Choi, D.-Y. Khang, Y. Huang, J. A. Rogers, *J. Appl. Phys.* **2008**, *103*, 014303.
- [23] C. M. Stafford, C. Harrison, K. L. Beers, A. Karim, E. J. Amis, M. R. Vanlandingham, H.-C. Kim, W. Volksen, R. D. Miller, E. E. Simonyi, *Nat. Mater.* **2004**, *3*, 545.
- [24] C. M. Stafford, B. D. Vogt, C. Harrison, D. Julthongpipit, R. Huang, *Macromolecules* **2006**, *39*, 5095.
- [25] A. J. Nolte, M. F. Rubner, R. E. Cohen, *Macromolecules* **2005**, *38*, 5367.
- [26] A. J. Nolte, R. E. Cohen, M. F. Rubner, *Macromolecules* **2006**, *39*, 4841.
- [27] E. A. Wilder, S. Guo, S. Lin-Gibson, M. J. Fasolka, C. M. Stafford, *Macromolecules* **2006**, *39*, 4138.
- [28] D.-Y. Khang, J. Xiao, C. Kocabas, S. MacLaren, T. Banks, H. Jiang, Y. Huang, J. A. Rogers, *Nano Lett.* **2008**, *8*, 124.
- [29] M. J. Schultz, X. Zhang, S. Unarunotai, D.-Y. Khang, Q. Cao, C. Wang, C. Lei, S. Maclaren, J. A. N. T. Soares, I. Petrov, J. S. Moore, J. A. Rogers, *Proc. Natl. Acad. Sci. USA* **2008**, *105*, 7353.
- [30] D. Takh, D.-Y. Khang, H. H. Lee, unpublished results.
- [31] H. Hoppe, N. S. Sariftci, *J. Mater. Chem.* **2006**, *16*, 45.
- [32] M. Campoy-Quiles, T. Ferenczi, T. Agnostonelli, P. G. Etchegoin, Y. Kim, T. D. Anthopoulos, P. N. Stavrinou, D. D. Bradley, J. Nelson, *Nat. Mater.* **2008**, *7*, 158.
- [33] S. P. Lacour, S. Wagner, Z. Huang, Z. Suo, *Appl. Phys. Lett.* **2003**, *82*, 2404.

- [34] S. Wagner, S. P. Lacour, J. Jones, P. I. Hsu, J. C. Sturm, T. Li, Z. Suo, *Physica E* **2004**, *25*, 326.
- [35] J. Jones, S. P. Lacour, S. Wagner, Z. Suo, *J. Vac. Sci. Technol, A* **2004**, *22*, 1723.
- [36] S. P. Lacour, J. Jones, S. Wagner, T. Li, Z. Suo, *Proc. IEEE* **2005**, *93*, 1459.
- [37] E. Menard, K. J. Lee, D.-Y. Khang, R. G. Nuzzo, J. A. Rogers, *Appl. Phys. Lett.* **2004**, *84*, 5398.
- [38] E. Menard, R. G. Nuzzo, J. A. Rogers, *Appl. Phys. Lett.* **2005**, *86*, 093507.
- [39] Y. Sun, D.-Y. Khang, F. Hua, K. Hurley, R. G. Nuzzo, J. A. Rogers, *Adv. Funct. Mater.* **2005**, *15*, 30.
- [40] D.-H. Kim, J.-H. Ahn, W. M. Choi, H.-S. Kim, T.-H. Kim, J. Song, Y. Huang, Z. Liu, C. Lu, J. A. Rogers, *Science* **2008**, *320*, 507.
-